Author Accepted Manuscript of paper accepted for publication in Railway Engineering Science, doi: 10.1007/s40534-025-00416-1

Assessing the impact of building foundations located in the transmission path on train-induced ground vibration using a hybrid computational model

Xiangyu Qu, David Thompson, Evangelos Ntotsios, Giacomo Squicciarini

Institute of Sound and Vibration Research, University of Southampton, Southampton SO17 1BJ, UK

Abstract

Train-induced ground vibration impacts the environment and has attracted increased attention. Prediction of this vibration is subject to considerable uncertainty and is affected by many factors, particularly when building foundations are situated within the transmission path between the vibration source and the target building. A hybrid computational model for predicting ground vibration has been developed to assess the impact of building foundations of various types located in the transmission path. The model is used to investigate four types of foundations: raft, strip, pile, and box. The ground responses are determined by combining the semi-analytical model MOTIV (**M**odelling **O**f **T**rain-**I**nduced **V**ibration) for train-induced vibration with a finite element model of the ground including the building. MOTIV is used to determine the excitation in terms of the force density for a train running either on a surface railway or in a tunnel. The finite element model is used to determine line source transfer mobilities in the presence of the building foundations by applying a set of incoherent unit loads to the ground. The results indicate that building foundations in the transmission path can mitigate ground vibration, particularly for excitation at the ground surface, for which reductions in overall vibration level of between 4 and

8 dB are found. Deep foundations provide greater vibration reduction than shallow foundations, notably in cases involving surface railways. The underground railway case demonstrates less significant insertion loss than the surface railway case, with values based on overall velocity level between -2 and 2 dB, rising to 4 dB for the box foundation. Furthermore, it is observed that ground vibration mitigation is more pronounced in the near field than in areas further from the building.

Keywords: train-induced vibration; ground vibration; hybrid model; finite element model; building foundation

1 Introduction

In recent years, rail transport has been increasingly recognised as an environmentally friendly and sustainable mode of transportation, helping to reduce traffic congestion and air pollution [1]. Railways provide notable environmental benefits in transporting both passengers and freight; however, train-induced ground vibration has become an issue of growing concern. A wide variety of prediction models, empirical, analytical and numerical, have been employed to predict train-induced ground vibration. Despite ongoing improvements in these prediction models, the ground is usually considered as a free field, whereas in reality there may be many other buildings between the vibration source (the track) and the target buildings (at which the vibration is to be assessed), or around the target building. Therefore, it is important to develop a prediction model that considers buildings located in the transmission path.

Empirical models [2-4], which may be based on measured data, theoretical or numerical predicted results, are relatively simple. The empirical method is usually used in the preliminary stage of environmental impact assessment and prediction, that is, in the initial feasibility study stage of the construction of a new railway line or

building. An example of an assessment of vibration mitigation based on measurements is given in [5]. The empirical method has relatively high prediction efficiency and low computational cost, but the prediction accuracy is relatively low if it is used for a situation other than the one where the measurements are taken. According to ISO 14837-1 [6], the prediction of vibration levels can be divided into three subproblems: the vibration source, the transmission path, and the receivers. The magnitude of ground-borne vibration at receivers can be represented as

$$A(f) = S(f)P(f)R(f) \tag{1}$$

where $S(f)$ is the source term, $P(f)$ represents the transmission path, $R(f)$ is the receiver term and f is frequency.

A commonly used empirical method is based on the procedures developed by the Federal Railroad Administration (FRA) and the Federal Transit Administration (FTA) in the USA [7, 8]. A chain formula is used that considers the three factors mentioned above expressed in decibels. There is an adjustment to account for ground-building foundation interaction and attenuation of vibration amplitude as vibration propagates through the target building. While most empirical models consider the influence of building foundations at the receiver, they do not adequately represent the impact of buildings situated in the transmission path on ground-borne vibration.

Analytical and numerical methods are also widely used to predict ground-borne vibration from trains. For example, Sheng et al. [9] produced a semi-analytical model of vibration from surface trains, while Hussein and Hunt predicted vibration from a train in a tunnel using the Pipe-in-pipe method [10], see also [11, 12]. Numerical methods include finite element and boundary element methods in 2D, 3D and 2.5D [13-19].

To predict train-induced vibration using (semi-)analytical or numerical methods, the building foundation (of the target building) is generally accounted for through the simulation of soil-structure interaction (SSI) effects. For use with the analytical method, the transfer matrix method [20] is widely applied. To compute the interaction force between the soil and the building foundation, the displacements of both are set

equal in order to satisfy the geometric compatibility conditions [21]. In addition, single-degree-of-freedom models [22], 2D framed models [23], and 3D analytical models [24, 25] are used to calculate building vibration induced by railways. Numerical methods such as the finite element method [26-31] and the boundary element method [32-35] are commonly employed to simulate the building foundation and SSI. These models are formulated in 2D [32], 3D [26, 28] and 2.5D [29-31] frameworks. However, most of these studies focus on receiver points located within the building, rather than in the area behind it. Therefore, the influence of the foundation on the ground needs further investigation when the building foundations are located in the vibration transmission path.

Hybrid methods have attracted increasing attention in recent years. The chain formula is too simplified for accurate prediction, whereas the reliability of numerical models and the accuracy of their prediction results depend on the accuracy of the input parameters. It is sometimes very difficult to obtain the physical parameters of the whole system with sufficient accuracy. Therefore, hybrid prediction models based on empirical methods combined with numerical methods are becoming popular. Verbraken et al. [36], and Kuo et al. [37] used such a hybrid empirical-numerical methodology to predict the ground vibration. This hybrid approach can use a combination of measured data, from train passages or from hammer excitation, and numerical models. Three cases can be considered: where both railway and target building are present, where the railway is present but there is no target building at the site, and where the target building is present but there is no track at the site. Kouroussis et al. [4, 38] predicted ground vibration in urban situations by combining the numerical and experimental methods, based on the framework of the FRA approach [7]. Colaço et al. [39] combined numerical results of the track–ground–building dynamic interaction system and experimental measurements of the vibration response and transfer mobilities to form a hybrid prediction model for the train-induced ground vibration. The SILVARSTAR European project [40] investigated the use of combinations of empirical and numerical models for the source and

transmission path terms in a hybrid prediction scheme. Although some building foundations and soil-structure interactions have been simulated using numerical approaches based on hybrid models, the buildings considered in these studies are all located as the receiver rather than elsewhere within the transmission path. Currently, limited research has been conducted on building foundations situated in the transmission path and their impact on ground vibration.

For the use of (semi) analytical methods or numerical methods, it is necessary to make simplifications, especially of the soil, which can affect the accuracy of vibration predictions. Moreover, reliable input parameters are required for the soil, including its layered structure, for which on-site measurements are necessary. Using such measurements directly in a hybrid modelling approach therefore has advantages. For example, Lai et al. [41] assessed the vibrational impact of underground railway traffic on two buildings in Rome by combining experimental measurements with numerical simulations. Liu et al. [42] predicted ground-borne vibration using a hybrid approach framework that includes an analytical train model for the source term and an in-situ measured transfer function for the transmission path term. Li et al. [43] predicted the vibration induced by an underground railway by using a hybrid model combining numerical modelling and experimental measurements. While measured transfer functions may describe the effects of particular building foundations in the vibration transmission path, it remains challenging to draw a general conclusion about the influence of various foundation types on ground vibration.

The presence of buildings within the transmission path cannot be overlooked. It is essential to investigate the influence of surrounding structures on ground-borne vibration induced by railways. In particular, the role of different building foundation types in modifying wave propagation should be thoroughly examined. In this work, a hybrid model following the FRA approach [7], but based on a combination of two different computational modelling methods, is proposed to assess the effect of different types of building foundation in the transmission path between the source and a receiver. The force density is calculated from a semi-analytical model, whereas the

transmission path is calculated from a numerical model; therefore, the proposed approach is called a hybrid computational model. This approach is taken to avoid the complication of including the different building foundations directly in the (analytical) train-track-ground model and to avoid including the train-track interaction in the FE model of the building. To maintain generality, the target building itself is not included in the model, with the receivers instead located on the ground surface. In Section 2, a semi-analytical model is introduced to calculate the force density levels from train passages. In Section 3, the line source transfer mobility is calculated from a numerical model that includes a building and its foundation in the transmission path. In Section 4, these are combined to determine the insertion loss results for a surface railway case and an underground railway case. The conclusions are summarised in Section 5.

2 Force density level

Based on the FRA approach [7], the ground vibration can be calculated by

$$L_{\mathrm{G}}(\mathbf{x}_{\mathrm{r}}) = L_{\mathrm{FD}}(\mathbf{X}) + L_{\mathrm{LSTM}}(\mathbf{X}, \mathbf{x}_{\mathrm{r}}) \tag{2}$$

where $L_{\mathrm{FD}}(\mathbf{X})$ is the force density level (FDL) describing the excitation due to train-track interaction, and $L_{\mathrm{LSTM}}(\mathbf{X}, \mathbf{x}_{\mathrm{r}})$ is the line source transfer mobility (LSTM) level describing the transmission path. Both are expressed in one-third octave bands in decibels. In the present work, the excitation in the form of the FDL is calculated using the train-track-tunnel-soil semi-analytical model MOTIV (**M**odelling **O**f **T**rain-**I**nduced **V**ibration) [44, 45].

2.1 MOTIV model

Two types of railway excitation are calculated using MOTIV: trains running on a surface railway and in an underground tunnel. The surface railway model includes the effects of the moving load [9] whereas the underground case uses a fixed train load position.

The surface railway model in MOTIV [9] encompasses sub-models for the train, track, and soil. The first step establishes the transfer function between a unit moving

harmonic load on the rail and the response of the ground, which is evaluated in the frequency-wavenumber domain. To allow for an arbitrary load distribution across the width of the track, the track-ground interface is discretised using a set of strips. In the second step the wheel-rail interaction force for a unit unevenness spectrum is calculated based on the receptances of the track and train. This force spectrum is then multiplied by the transfer function to compute the ground response induced by the moving train. The dynamic response is finally calculated by combining this result with the rail roughness spectrum. Additionally, the quasi-static ground response to moving constant axle loads is calculated; the total ground response is the sum of the quasi-static and dynamic responses.

The underground railway model in MOTIV is based on the pipe-in-pipe approach [46-48] and includes sub-models for the train, track, tunnel, and soil. The following steps are required to calculate the ground response: (1) the displacement is computed in the frequency-wavenumber domain of a circular tunnel embedded in a full-space due to a vertical harmonic load applied at the tunnel invert. (2) A model of a full space (without a tunnel) is next considered. A set of equivalent loads in the full space is determined, that produces the same displacement at the tunnel-soil interface as computed in the first step. (3) A model of a multi-layered half-space without a tunnel is considered, and the ground response due to the equivalent loads from the second step is calculated using the dynamic stiffness matrix method. (4) The track is coupled to the tunnel using the equilibrium of displacements between the tunnel invert and the track. (5) The train is coupled with the track, excited by the unevenness. For computational efficiency, the underground railway model omits both moving loads and the quasi-static component. This corresponds to a low-speed approximation, which is assessed in [40] and shown to have a relatively small influence, apart from some redistribution of energy into neighbouring frequency bands, provided that the train speed remains much lower than the wave speeds in the soil.

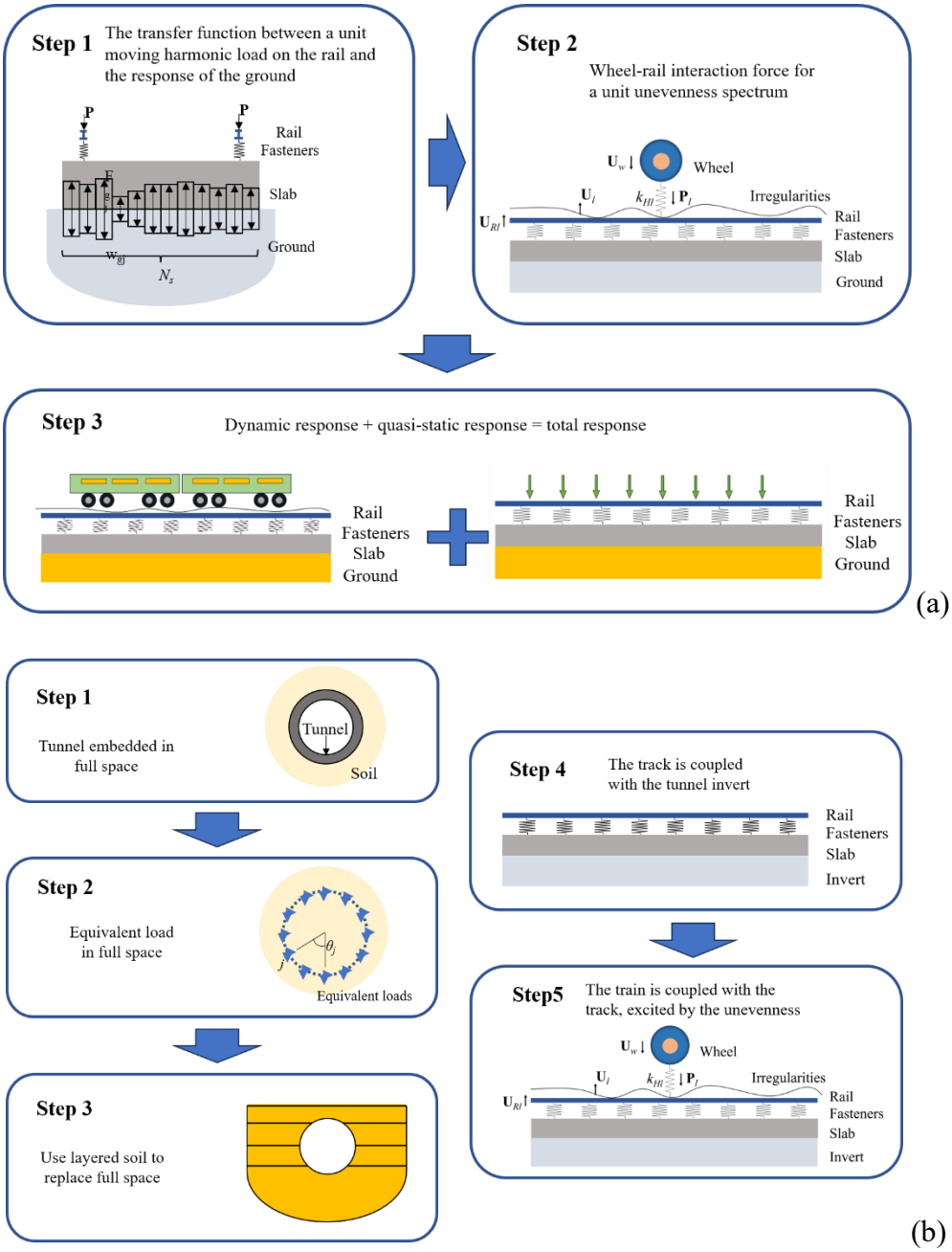

Figure 1 Schematic diagram of the (a) surface railway model and (b) underground railway model.

Using these models, the FDL beneath the trackbed is derived from the ground response during a train pass-by. In the MOTIV model, the trackbed and the tunnel/ground are directly coupled, making it difficult to obtain the FDL directly. Therefore, the FDL is determined indirectly by subtracting the LSTM from the ground

response. The FDLs from both models are calculated by using equation (1) in reverse:

$$L_{\mathrm{FD}}(\mathbf{X}) = L_{\mathrm{G}}(\mathbf{x}_{\mathrm{r}}) - L_{\mathrm{LSTM}}(\mathbf{X}, \mathbf{x}_{\mathrm{r}}) \tag{3}$$

where $L_{\mathrm{G}}(\mathbf{x}_{\mathrm{r}})$ is the ground response velocity level at the receiver position $\mathbf{x}_{\mathrm{r}}$ during a train pass-by, calculated from the semi-analytical model for either the underground railway or surface railway case. $L_{\mathrm{LSTM}}(\mathbf{X}, \mathbf{x}_{\mathrm{r}})$ is the LSTM level at $\mathbf{x}_{\mathrm{r}}$ when the excitation positions are at $\mathbf{X}$. This LSTM level is calculated from the semi-analytical model using the same parameters as the pass-by calculations.

The LSTM can be determined by combining a set of transfer mobilities obtained for these point loads. The LSTM for the line load excitation at position $\mathbf{X}$ can be calculated by [7, 8]

$$Y_{\mathrm{L}}(\mathbf{X}, \mathbf{x}_{\mathrm{r}}) = \sqrt{\frac{L}{n}\sum_{i=1}^{n} |Y_i(\mathbf{x}_i, \mathbf{x}_{\mathrm{r}})|^2} \tag{4}$$

where L is the length of the line load, n is the number of incoherent point loads, $Y_i(\mathbf{x}_i, \mathbf{x}_{\mathrm{r}})$ is the transfer mobility from the point load applied at position $\mathbf{x}_i$ to the receiver position $\mathbf{x}_{\mathrm{r}}$. The LSTM level in decibels (with reference value 1 $\mathrm{m^{3/2}N^{-1}s^{-1}}$) is written as

$$L_{\mathrm{LSTM}}(\mathbf{X}, \mathbf{x}_{\mathrm{r}}) = 20\log_{10}\big(Y_{\mathrm{L}}(\mathbf{X}, \mathbf{x}_{\mathrm{r}})\big) \tag{5}$$

In the FRA approach [7] the FDLs can be determined at the track, or at the track-ground interface, depending on whether the railway is present at the target site. This choice determines the location of the excitation positions used to obtain the LSTM. Considering the application of the force densities in Section 3, the FDL is required for excitation on the ground surface for the surface railway case, and for excitation on the track slab for the underground railway case. These positions are therefore chosen for the forces in the corresponding LSTM calculation here. For the surface railway case, an incoherent line load is applied on the ground surface, while for the underground railway case, an incoherent load is applied on the invert. The distance between point loads is 9 m. In these models, the ground response receiver point $\mathbf{x}_{\mathrm{r}}$ used for determining the FDL is located on the ground surface at a horizontal distance of 8 m

away from the railway centreline.

2.2 Model parameters

A consistent set of parameters and properties for the train, track, and soil are used for both the surface and underground railway cases. The parameters of the train (representing a typical InterCity train) are summarised in Table 1 [49]. The train speed is 60 km/h. The parameters of the track are summarised in Table 2 [49]. The track type is taken as a slab track for both cases. The tunnel structure parameters used for the underground railway case are summarised in Table 3. The soil parameters for both cases are summarised in Table 4.

Table 1 Parameters of the train [49].

Property	**Value**	**Unit**
Vehicle length	23	m
Bogie wheelbase	2.5	m
Bogie centre distance	17	m
Vehicle body mass	32000	kg
Vehicle pitching moment of inertia	1.2×10^{6}	kgm^2
Bogie mass (without axles)	5000	kg
Bogie pitching moment of inertia	6000	kgm^2
Wheelset mass	1200	kg
Static axle load	1.148×10^{5}	N
Contact stiffness (per wheel)	1.13×10^{9}	N/m
Primary suspension stiffness (per axle)	2.0×10^{6}	N/m
Primary suspension damping (per axle)	4×10^{4}	Ns/m
Secondary suspension stiffness (per car end)	5×10^{5}	N/m
Secondary suspension damping (per car end)	3.16×10^{4}	Ns/m

Table 2 Track model parameters [49].

	Property	**Value**	**Unit**
Rail, UIC 60	Bending stiffness	6.42×10^{6}	Nm^2
	Mass per unit length	60	kg/m
	Damping loss factor	0.01	-
Rail pad	Stiffness	1.20×10^{8}	N/m
	Damping loss factor	0.15	-
	Fastener spacing	0.65	m
Slab	Width (at base)	3.4	m
	Height	0.54	m
	Mass per unit length	3720	kg/m
	Bending stiffness	2.33×10^{8}	Nm^2
	Damping loss factor	0.015	-
	Torsional stiffness	3.39×10^{8}	Nm^2
	Polar moment of inertia	3086	kgm

Table 3 Parameters of the tunnel structure.

Property	**Value**	**Unit**
External radius	3.0	m
Thickness of tunnel wall	0.3	m
Density	2500	kg/m^3
Young's modulus	5×10^{10}	N/m^2
Poisson's ratio	0.3	-
Mass per unit length for invert	2500	kg/m
Bending stiffness for invert	1×10^{8}	Nm^2
Loss factor for tunnel and invert	0.02	-
Depth of tunnel centre	10	m

Table 4 Parameters of the soil.

Materials	**Property**	**Value**	**Unit**
Concrete	Density	2500	kg/m^3
	Young's modulus	3×10^{10}	N/m^2
	Poisson's ratio	0.2	-
	Loss factor	0.1	-
	P-wave velocity	3652	m/s
	S-wave velocity	2236	m/s
Soil	Density	2100	kg/m^3
	Young's modulus	3.5×10^{8}	N/m^2
	Poisson's ratio	0.333	-
	Loss factor	0.1	-
	P-wave velocity	500	m/s
	S-wave velocity	250	m/s

To represent a typical unevenness spectrum, the "normal slab track roughness" obtained from the SILVARSTAR database is used [50]. The roughness levels at different wavelengths in one-third octave bands are plotted in Figure 2 in dB re 10^{-6} m.

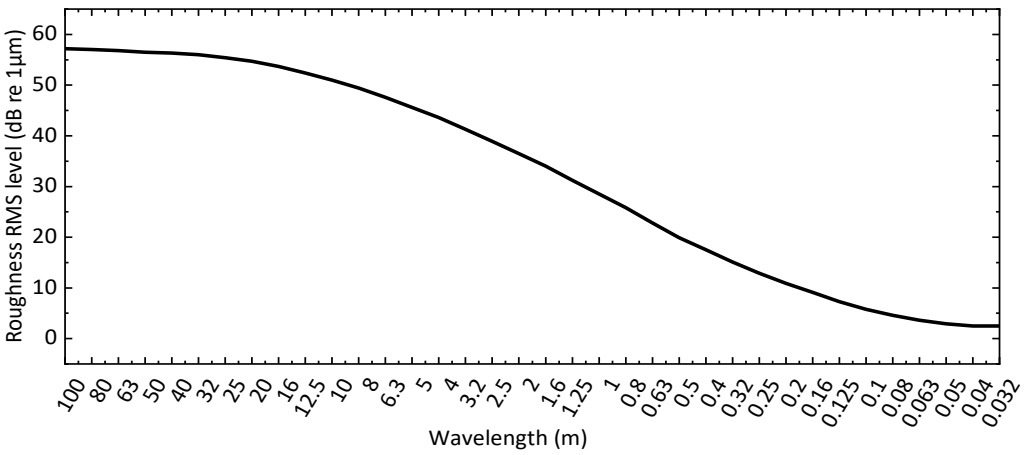

Figure 2 The track roughness spectrum in one-third octave bands.

2.3 Force density level results

The FDLs for the surface railway case and the underground railway case are shown in Figure 3. There is a significant peak at 50 Hz in both cases, which corresponds to the P2 resonance at which the vehicle unsprung mass bounces on the track stiffness [51]. The FDL of the surface railway case is smaller than that from underground railway case. The difference occurs due to the difference in excitation positions.

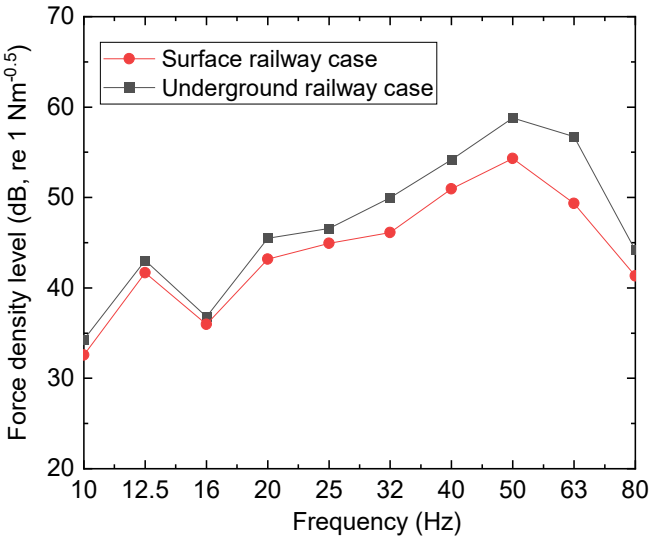

Figure 3 Force density levels for an InterCity train running at 60 km/h on a slab track on a surface railway or in a tunnel. For the surface railway the force is applied to the ground surface whereas for the underground railway case it is applied to the tunnel invert.

3 Line source transfer mobility level

To determine the ground response including building foundations, the LSTM is calculated using 3D finite element (FE) models constructed in ABAQUS. In contrast to the analytical model, the FE model can account for foundations with varying shapes and geometries, enabling a more accurate representation of their influence on ground vibration. This capability makes the FE model a suitable choice for computing the LSTM. The models encompass the soil and a building structure, complete with foundations; the track is not included in these models. A sketch of the surface excitation model is shown in Figure 4(a).

In the underground excitation model, the tunnel structure is additionally embedded in the surrounding soil, but again the track is omitted. A sketch of the underground excitation model is shown in Figure 4(b). The model dimensions, element sizes, and material properties remain consistent with those of the surface excitation model, as described in the following section.

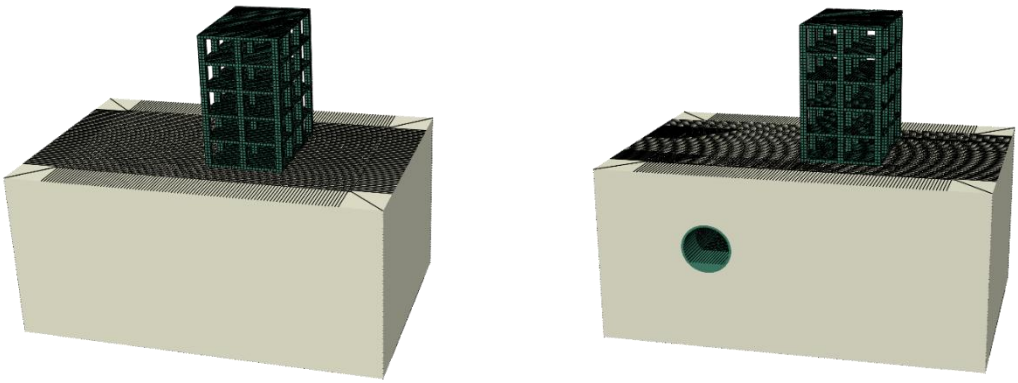

(a) (b)

Figure 4 Sketch of (a) surface excitation and (b) underground excitation FE model in ABAQUS.

3.1 Model parameters

The building structures and their foundations, as well as the tunnel structure, are indicated by the green elements in Figure 4. They are assumed to be constructed from concrete. The soil is shown in cream colour. The soil properties are the same as those listed in Table 4. The properties used for the concrete are also listed in Table 4.

The dimensions of the two models are 50 m×34 m, with a depth of 24 m. For the underground excitation case, as in Section 2, the outer diameter of the tunnel is 6 m, and the thickness of the tunnel wall is 0.3 m. The depth of the tunnel centre is 10 m.

In these ABAQUS models, the element type is designated as C3D8, denoting a three-dimensional, eight-node brick element. Infinite elements are applied on the side boundaries of the soil domain, to minimise the wave reflections. The bottom of the FE models is fixed. The horizontal distance between the loads and the front of the building is 10 m in each case. Receiver points are designated within an area measuring 17.6 m by 8.4 m, located immediately behind the building structure. The spacing between the receiver points in the grid is 0.4 m. The boundary conditions and the positions of an example point load and the receiver points are indicated in Figure 5.

In each model, the building encompasses five storeys, configured in a layout of 3

× 2 bays. Each storey has a height of 3.2 m, and each bay has a span width of 4.8 m. The thickness of the floor is 0.4 m, and the columns have a square cross-section with dimensions 0.8 m by 0.8 m. The side walls are omitted.

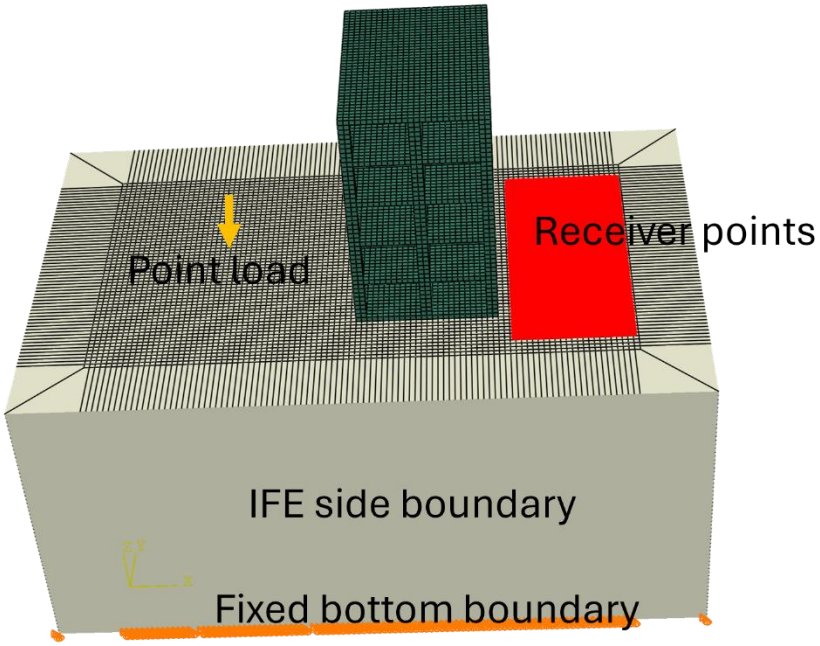

Figure 5 The boundary conditions, load and receiver positions in the FE model for surface excitation.

There are a total of 360,000 elements for the underground excitation model and 373,000 elements for the surface excitation model. The maximum element size is set at 0.4 m. For the shear wave velocity of 250 m/s, this is sufficient to satisfy the usual requirement that there are at least six elements within one wavelength for frequencies up to 100 Hz.

To determine the LSTM, a set of incoherent point loads is applied. As the model is symmetric, 10 incoherent loads are applied in the model on one side of the centreline, as shown in Figure 6. For the surface railway case, these loads are applied on the ground surface, whereas for the underground railway case, they are applied on the invert of the tunnel. The interval between these loads is 1.2 m in each case. The FE models are calculated in the frequency domain.

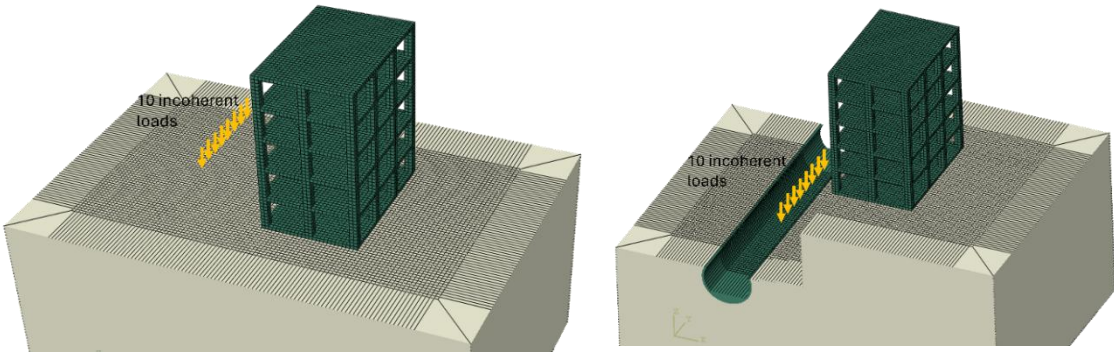

(a) (b)

Figure 6 Sketch of incoherent loads for (a) surface excitation case and (b) underground excitation case.

As verification, Figure 7 presents a comparison of the free-field LSTM responses between the FE model (without the building) and the semi-analytical model MOTIV calculated from Eqs. (4) and (5). The LSTM spectrum is shown for a receiver on the centreline, located 26 m from the line load. Although differences in model size, incoherent line length, and load spacing lead to some differences in these results, both models exhibit similar overall trends, with a maximum difference of less than 3 dB.

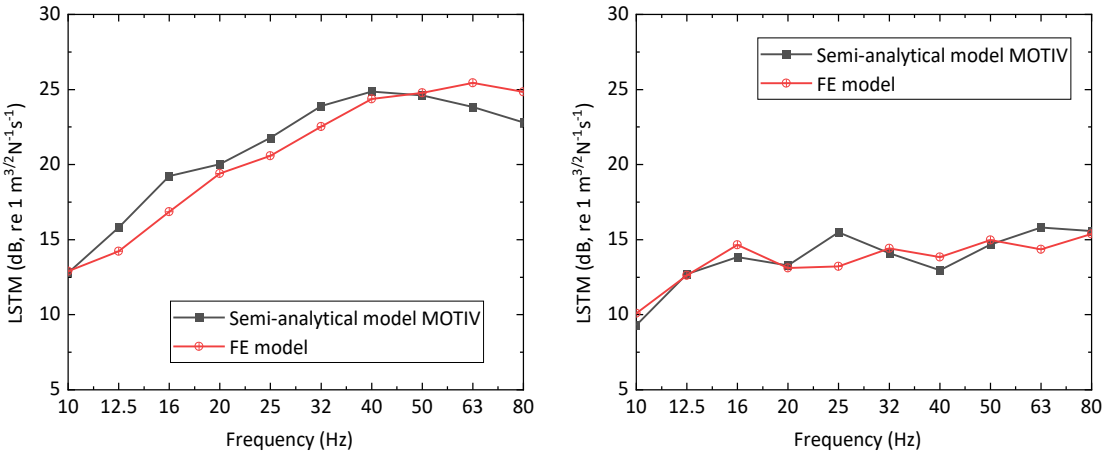

(a) (b)

Figure 7 Comparison of the free field LSTM between FE model and MOTIV when loads are applied (a) on the ground surface and (b) on the tunnel invert.

3.2 Foundation types

The influence of different building foundation types in the transmission path is

investigated using the FE models. Four common foundation types are summarised in reference [52]. Two are shallow foundations, the pad/strip foundation and the raft foundation, while the others are deep foundations, the piled foundation and embedded basement foundation.

FE models representing these four different foundation types have been created in ABAQUS and are shown in Figure 8. Additionally, a model with no building is considered as a reference case.

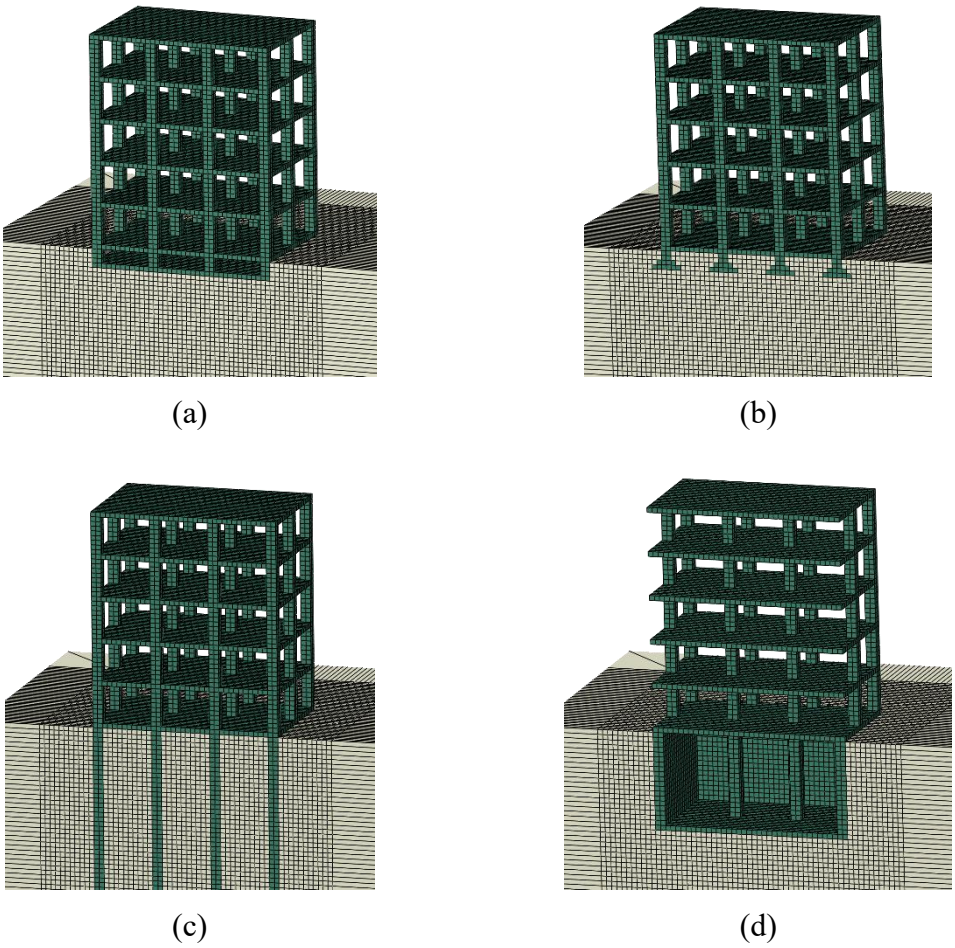

Figure 8 The profile of structures with different foundation types: (a) raft foundation, (b) strip foundation, (c) pile foundation, and (d) box foundation.

Figure 8(a) shows the raft foundation. There are 12 small columns with height 1.2 m beneath the ground surface. The area of the raft is $10.4 \times 15.2 = 158.08$ m^2. Figure 8(b) shows the strip foundation. The height of each strip is 1.6 m. The strip foundation is implemented with two orientations: one normal to the direction of the

train passage (denoted 'StripN' shown in Figure 8(b)), and the other tangential to it (denoted 'StripT'). In each case the length of the strip is commensurate with the building's dimensions. Figure 8(c) shows the pile foundation. There are 12 piles in this model, with a depth of 10 m. Finally, Figure 8(d) shows the box foundation. The height of the box is 8 m, and the thickness of the walls is 0.8 m. It contains two internal columns.

3.3 Average results from receiver points at the same distance

The LSTM is determined for the grid of receiver points indicated in Figure 5. To summarise the results, the average LSTM value from all the receiver points at the same distance behind the building is calculated by

$$L_{\mathrm{LSTM,average}}^{\mathrm{building}}(y,\omega) = 10\log_{10}\left(\frac{1}{K}\sum_{k=1}^{K} 10^{\frac{L_{\mathrm{LSTM}}^{\mathrm{building}}(\mathbf{y}_{\mathrm{r}}^{k},\omega)}{10}}\right) \tag{6}$$

where $L_{\mathrm{LSTM}}^{\mathrm{building}}(\mathbf{y}_{\mathrm{r}}^{k},\omega)$ means the LSTM from the numerical model including the building at the k-th receiver point $\mathbf{y}_{\mathrm{r}}^{k}$ at distance y. The results are expressed in one-third octave bands with central frequency ω. Within each one-third octave band, three frequency points are used for computation.

The average LSTM results from all the receiver points over ± 8.8 m width at an example distance of 5.6 m away from the rear of the building (26 m away from the location of the railway track) are shown in Figure 9. Results are shown for the incoherent loads applied on the ground surface or on the tunnel invert. The calculation is based on Eq. (6). The differences between the free-field response and the foundation cases for underground load case are much smaller than the differences in the surface load case. When the incoherent loads are applied on the ground surface, the free-field response is larger than in the presence of the building for frequencies above 20 Hz. The box foundation case shows the lowest LSTM level results. When the incoherent loads are applied on the tunnel invert, the trend across all foundation types is similar to that for the surface loads, although the values of LSTM in the underground load cases are around 5 dB lower than those in the surface load cases due to the incoherent load being embedded at depth. Unlike the surface load case, the

results without the building are similar to those with different building foundations.

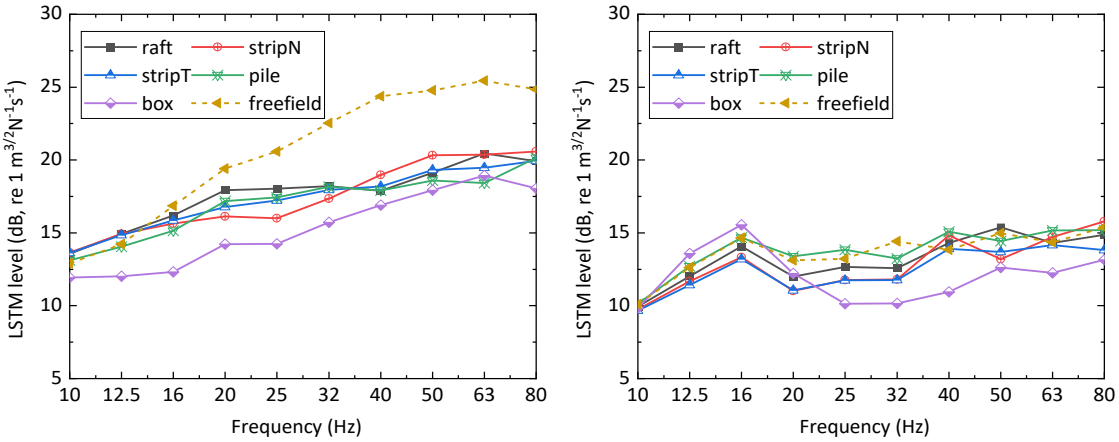

(a) (b)

Figure 9 The average LSTM level from all the receivers 5.6 m away from the rear of the building excited (a) on the ground surface and (b) in the tunnel.

4 Ground response for different foundation types

According to the adopted hybrid computational methodology, the ground vibration due to a passing train can be calculated from Eq. (2), by combining the FDL and LSTM calculated above. Results are presented for each of the five foundation types introduced in Section 3.2.

4.1 Surface railway case

4.1.1 Spectral results

To summarise the effect of each building foundation, the average insertion loss (IL) spectrum is calculated for all the receiver points at the same distance behind the building. The average ground velocity level at distance y behind the building is first calculated by

$$L_{\mathrm{G,average}}^{\mathrm{building}}(y,\omega) = 10\log_{10}\left(\frac{1}{K}\sum_{k=1}^{K} 10^{\frac{L_{\mathrm{G}}^{\mathrm{building}}(\mathbf{y}_{\mathrm{r}}^{k},\omega)}{10}}\right) \tag{7}$$

where $L_{\mathrm{G}}^{\mathrm{building}}(\mathbf{y}_{\mathrm{r}}^{k},\omega)$ means the ground vibration level at the k-th receiver point $\mathbf{y}_{\mathrm{r}}^{k}$

at distance y. The results are expressed in one-third octave bands with central frequency ω.

Similarly, the average ground vibration level in the free field at distance y is calculated by

$$L_{\mathrm{G,average}}^{\mathrm{free}}(y,\omega) = 10\log_{10}\left(\frac{1}{K}\sum_{k=1}^{K} 10^{\frac{L_{\mathrm{G}}^{\mathrm{free}}(\mathbf{y}_r^k,\omega)}{10}}\right) \tag{8}$$

where $L_{\mathrm{G}}^{\mathrm{free}}(\mathbf{y}_r^k,\omega)$ represents the ground vibration level from the free-field model at the k-th receiver point $\mathbf{y}_r^k$ at distance y. The results are again expressed in one-third octave bands.

The average value of IL at a distance y behind the building can be calculated from these results by

$$IL_{\mathrm{average}}(y,\omega) = L_{\mathrm{G,average}}^{\mathrm{free}}(y,\omega) - L_{\mathrm{G,average}}^{\mathrm{building}}(y,\omega) \tag{9}$$

The IL spectrum from the surface railway case is shown in Figure 10 for receiver points located 5.6 m behind the building. The IL is positive for all cases for frequencies above 16 Hz, rising to values between 4 and 7 dB above 32 Hz, indicating that regardless of the foundation type, the building can reduce the ground vibration behind it. The box foundation model typically achieves the largest IL values, especially at frequencies below 50 Hz, whereas the raft foundation case exhibits the lowest IL values at frequencies below 32 Hz. The stripN case shows moderate IL values at frequencies below 32 Hz, but it gives the lowest values at frequencies of 40 Hz and above. The pile and stripT cases display similar trends at lower frequencies but there is a notable peak in the IL for the pile foundation case at 63 Hz.

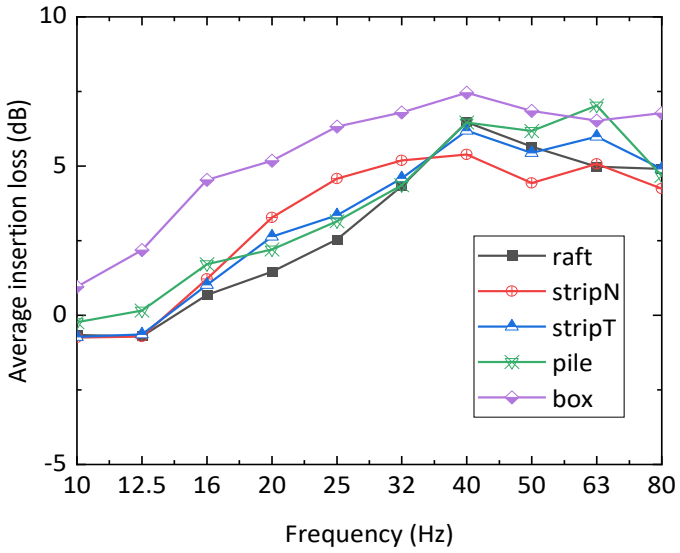

Figure 10 The average insertion loss results from all receivers 5.6 m away from the building excited by the surface railway.

4.1.2 Results based on overall levels

The overall ground velocity level behind the building due to the train passage is calculated by a sum over one-third octave bands.

$$L_{\mathrm{G,overall}}^{\mathrm{building}}(\mathbf{y}_{\mathrm{r}}) = 10\log_{10}\left(\sum_{i=1}^{n} 10^{\frac{L_{\mathrm{G}}^{\mathrm{building}}(\mathbf{y}_{\mathrm{r}},\omega_i)}{10}}\right) \tag{10}$$

where $L_{\mathrm{G}}^{\mathrm{building}}(\mathbf{y}_{\mathrm{r}},\omega_i)$ means the ground response velocity level in the i-th one-third octave band. The frequency range covers bands from 10 Hz to 80 Hz, since the ground vibration below 10 Hz is not significantly influenced by the presence of the building foundation, and does not significantly contribute to the overall vibration level.

The overall ground response velocity level in the free field is similarly calculated by

$$L_{\mathrm{G,overall}}^{\mathrm{free}}(\mathbf{y}_{\mathrm{r}}) = 10\log_{10}\left(\sum_{i=1}^{n} 10^{\frac{L_{\mathrm{G}}^{\mathrm{free}}(\mathbf{y}_{\mathrm{r}},\omega_i)}{10}}\right) \tag{11}$$

where $L_{\mathrm{G}}^{\mathrm{free}}(\mathbf{y}_{\mathrm{r}},\omega_i)$ represents the ground response velocity level from the free-field model in the i-th one-third octave band.

An overall value of IL at receiver points $\mathbf{x}_{\mathrm{r}}$ can be calculated by

$$IL_{\text{overall}}(\mathbf{y}_\text{r}) = L^{\text{free}}_{\text{G,overall}}(\mathbf{y}_\text{r}) - L^{\text{building}}_{\text{G,overall}}(\mathbf{y}_\text{r}) \tag{12}$$

The overall IL results at each receiver point over a region behind the building on the ground surface are shown as contour plots in Figure 11 corresponding to the various types of foundation. The approximate building position is also marked in these figures.

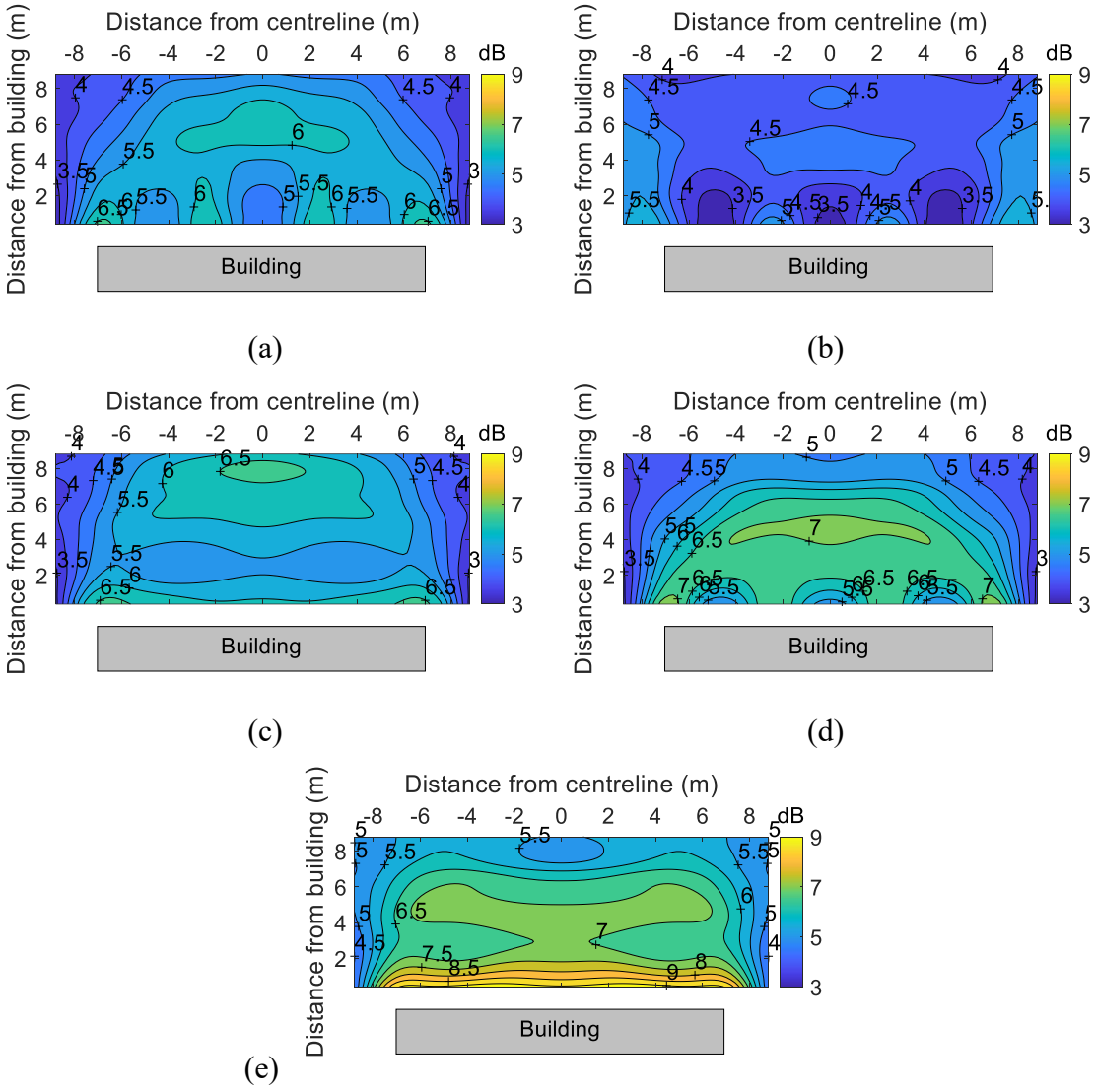

Figure 11 Contour plots of overall IL on the ground behind different types of building foundation for surface railway excitation: (a) raft foundation (b) strip foundation in normal direction (c) strip foundation in tangential direction (d) pile foundation and (e) box foundation.

For the shallow foundations, raft and strip (normal direction), as well as the pile foundation case, higher values of IL are observed in proximity to the building. This is

particularly evident near the columns of the building, where the IL values exceed those of the surrounding regions. As the distance between the receiver point and the building increases, there is a gradual decrease in the IL values. Nonetheless, certain specific areas exhibit local maxima. For the strip foundation oriented tangentially to the train's movement, an isolated zone of increased IL is observed between 4 m to 8 m away from the building. In the case involving the building with the box foundation, a larger area of increased IL is discernible in the vicinity of the building, along with a pronounced trend of reducing IL at greater distances from the building.

4.1.3 Overall results averaged over receiver points

The average overall IL value from all the receiver points at the same distance behind the building is also calculated using the same procedure. The average overall ground velocity value level at distance y behind the building is calculated by

$$L_{\mathrm{G,average}}^{\mathrm{building}}(y) = 10\log_{10}\left(\frac{1}{K}\sum_{k=1}^{K} 10^{\frac{L_{\mathrm{G,overall}}^{\mathrm{building}}(\mathbf{y}_{\mathrm{r}}^{k})}{10}}\right) \tag{13}$$

where $L_{\mathrm{G,overall}}^{\mathrm{building}}(\mathbf{y}_{\mathrm{r}}^{k})$ means the overall ground response velocity level (i.e. the sum over frequency bands) including the building at the k-th receiver point $\mathbf{y}_{\mathrm{r}}^{k}$ at distance y, calculated by using Eq. (10).

The equivalent level in the free field is similarly calculated by

$$L_{\mathrm{G,average}}^{\mathrm{free}}(y) = 10\log_{10}\left(\frac{1}{K}\sum_{k=1}^{K} 10^{\frac{L_{\mathrm{G,overall}}^{\mathrm{free}}(\mathbf{y}_{r}^{k})}{10}}\right) \tag{14}$$

where $L_{\mathrm{G,overall}}^{\mathrm{free}}(\mathbf{y}_{r}^{k})$ represents the overall ground response velocity level from the free-field model at the k-th receiver point at distance y, calculated by using Eq. (11).

The average value of IL at a distance y behind the building can be calculated by

$$IL_{\mathrm{average}}(y) = L_{\mathrm{G,average}}^{\mathrm{free}}(y) - L_{\mathrm{G,average}}^{\mathrm{building}}(y) \tag{15}$$

The overall ground velocity response results are averaged over ±8.8 m width for each specific distance from the rear of the building, covering a range from 1.2 m to

9.6 m. Based on Eqs. (13) and (14), the ground velocity levels for the five different foundation cases, along with the free-field response, are shown in Figure 12(a). For all foundation cases, the ground response is lower than the free-field response level. As the distance from the building increases, the ground response in the free field decreases and a similar trend is observed for all foundation types apart from the box foundation. Of the different foundation types, the box foundation typically exhibits the lowest response, while the stripN case generally gives the highest.

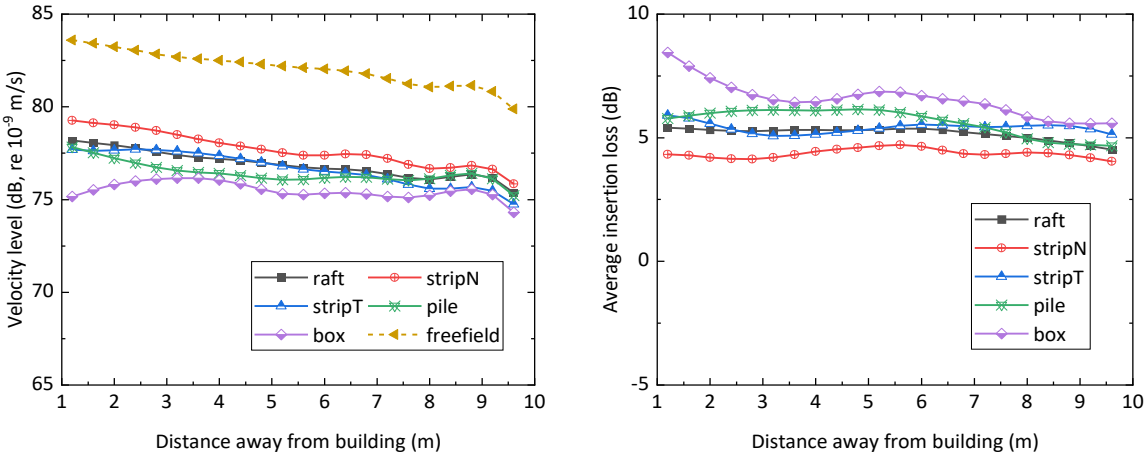

(a) (b)

Figure 12 (a) Ground velocity level and (b) IL determined from overall level, averaged over ±8.8 m width and plotted against distance from the building (surface railway case).

Figure 12(b) shows the corresponding IL values calculated from the average velocity levels at positions equidistant from the building structure, based on Eq. (15). These values of IL range from 4 to 6 dB, rising to 8 dB for the box foundation at positions close to the building. The box foundation consistently gives the largest values of IL, irrespective of the distance from the building. When the strip foundation is oriented perpendicular to the track, it exhibits the lowest IL value among all the cases. Overall, the results indicate that for shallow foundations, i.e. raft and strip foundations, the average IL values are lower than those observed for deep foundations, i.e., pile and box foundations. In the case of strip foundations, when the orientation of the strip is normal to the track (stripN), the IL is lower than when it is aligned tangentially (stripT). At 3-5 m away from the building, the IL values for the stripT

case are as low as those from the raft case. However, the stripT case exhibits a higher IL than the pile case for distances greater than about 7 m.

4.2 Underground railway case

4.2.1 Spectral results

For the underground railway case, Figure 13 shows the IL spectra obtained from the average responses of all the receiver points located 5.6 m away from the building, calculated according to Eqs.(7) to (9). The box foundation exhibits the lowest IL values at lower frequencies, but at frequencies above 25 Hz it displays the highest values compared to other types of foundation. The pile foundation exhibits the lowest IL values (apart from 12.5 Hz and 16 Hz), differing from the surface railway case. At certain frequencies, notably 40 Hz and 63 Hz, the IL value is negative, indicating that the response may be amplified due to the presence of the pile foundation building. In the region 10–32 Hz, the strip foundation yields similar ground vibration mitigation effects regardless of the orientation of the strip. The raft foundation exhibits a moderate reduction in ground vibration.

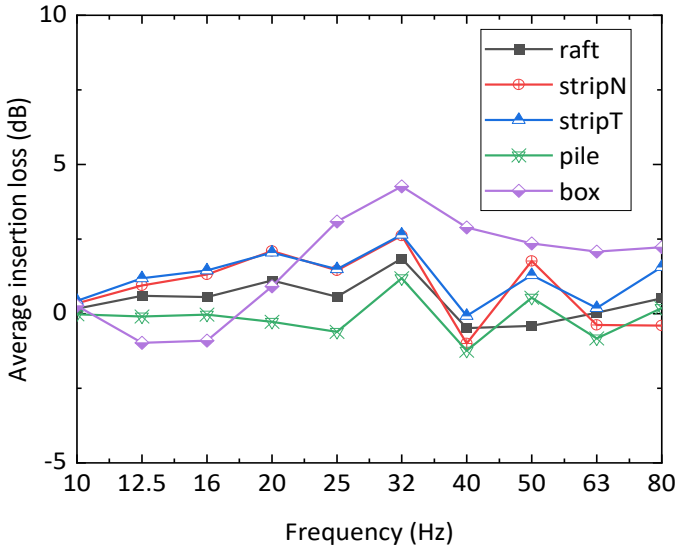

Figure 13 The average insertion loss results from all the receivers 5.6 m away from the rear of the building excited by underground railway.

4.2.2 Results based on overall levels

The contour plots of the overall IL value, i.e. based on the level difference in overall velocity levels calculated using Eq. (12), are shown in Figure 14.

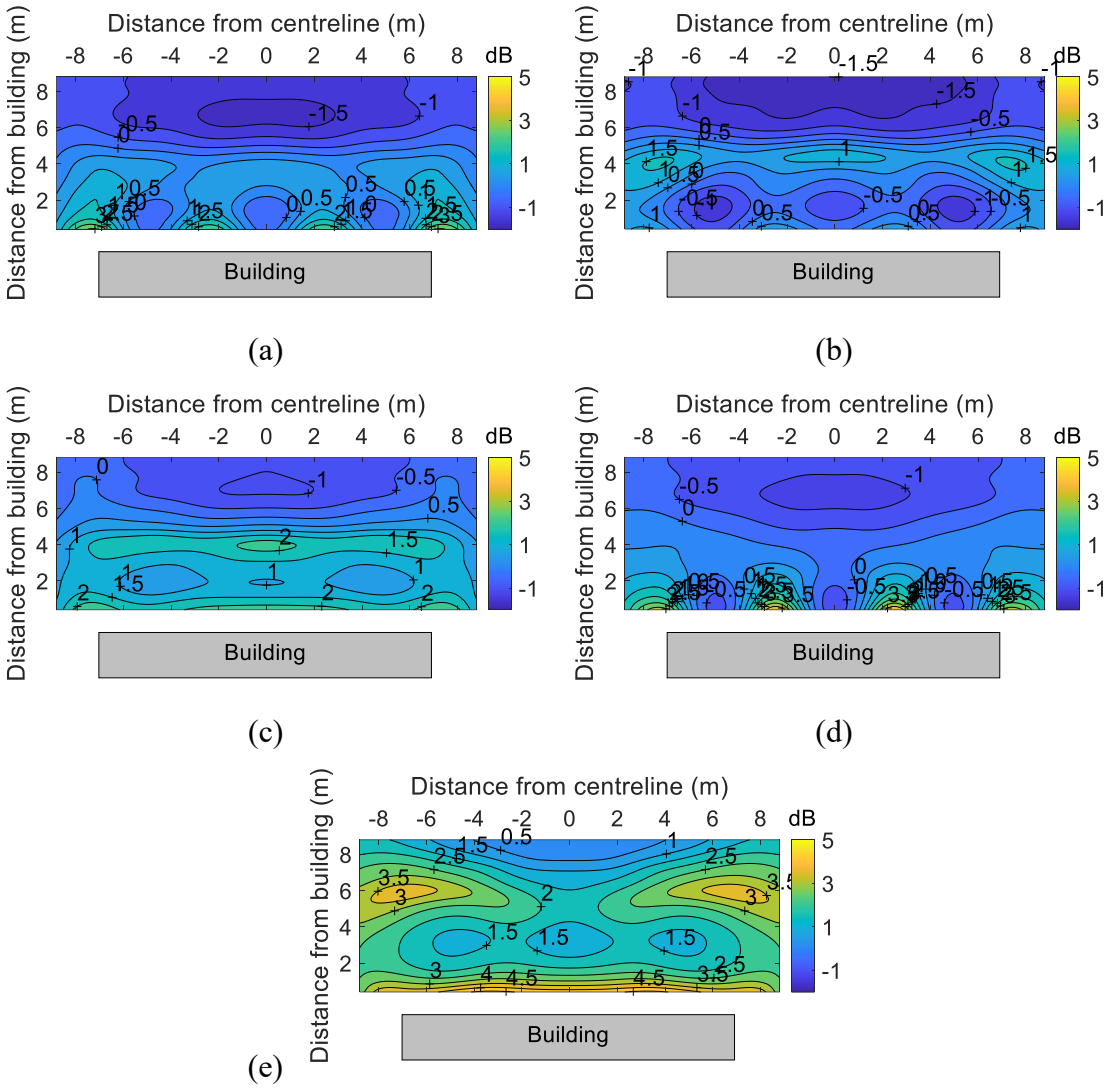

Figure 14 Contour plots of IL on the ground behind different types of building foundation for underground railway excitation: (a) raft foundation (b) strip foundation in normal direction (stripN) (c) strip foundation in tangential direction (stripT) (d) pile foundation and (e) box foundation.

In the case of the underground railway, the IL contours display more erratic patterns than for the surface railway and the overall levels of IL are smaller. The stripT foundation tends to give higher IL values in the proximity of the building. Also, for the building with the box foundation, the values of IL in areas close to the building are relatively high compared with other locations. For raft and pile foundations, the

columns influence the ground vibration in their vicinity. Typically, for all the building foundations there are regions of both ground vibration mitigation and amplification.

4.2.3 Overall results averaged over receiver points

Figure 15 shows the overall ground velocity response and IL results averaged over ±8.8 m width for each specific distance from the rear of the building, covering a range from 1.2 m to 9.6 m. The results are calculated using Eqs. (13) to (15) and are presented for the five different foundation cases, along with the free-field response. As before, the overall ground velocity levels are evaluated over the frequency range 10 Hz to 80 Hz.

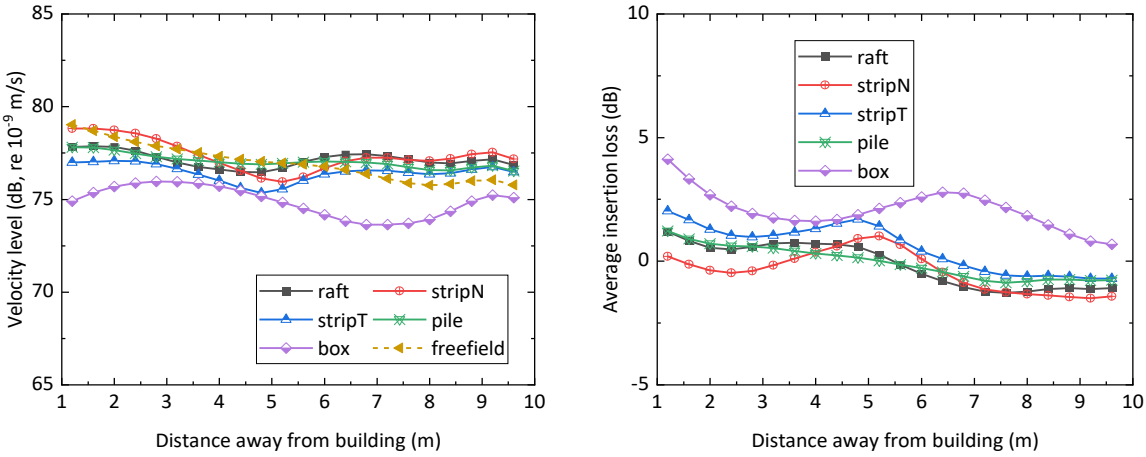

(a) (b)

Figure 15 The average (a) ground velocity level and (b) IL at different distances averaged over ±8.8 m width, plotted against distance from the building (underground railway case).

In Figure 15(a), it is evident that the box foundation consistently gives the lowest ground response across all distances. Conversely, the strip foundation oriented perpendicular to the track gives the largest ground response in the near field. The ground response for the raft foundation case and pile foundation case are similar to the free-field response.

These results are shown in the form of IL in Figure 15(b). The box foundation gives the largest vibration mitigation, as also found in the surface railway case in Figure 12; here the reduction is between 1 and 4 dB. However, in the underground railway case, all the other foundation types have similar values of IL, which are much

smaller than for the surface railway, and fall in the range ±2 dB. The strip foundations give some vibration attenuation at the ground surface behind the building, particularly at certain distances where the IL has a peak. The positions of these IL peaks are influenced by the orientation of the strip foundation. Pile foundations do not have a more significant vibration mitigation effect compared to shallow foundations, unlike in the surface railway case. At distances greater than about 6 m, all the foundations apart from the box give negative values of average IL, as also seen in Figure 14.

5 Conclusions

A hybrid ground vibration prediction model is used to assess the impact of various types of building foundations located in the transmission path on ground vibration due to passing trains. This approach separates the modelling of the building from that of the train pass-by and readily allows assessment of different foundation types. Five types of building foundations are considered: strip foundations (in two orientations) and raft foundations, which are shallow foundations; and pile foundations and box foundations, which are deep foundations. These models clearly illustrate the influence of foundation type on ground vibration. The IL value at the ground surface in proximity to the building is investigated. The following conclusions can be drawn:

1. From this computational hybrid model, it can be concluded that the presence of a building foundation in the transmission path can reduce ground vibration, especially for excitation at the ground surface. The deep foundations have greater vibration mitigation effects than the shallow foundations, especially for the surface railway case.
2. Additionally, it is observed that ground vibration mitigation is more pronounced in the near field compared with the results obtained further away from the building.

3. When examining the ground response results for different foundation types, the IL values for the surface railway case are generally larger than those for the underground railway case, with IL based on overall velocity level between 4 and 8 dB.
4. For the surface railway case, the IL is positive above 16 Hz, regardless of the foundation type. The box foundation consistently produces the highest IL value for both surface and underground railways.
5. For the underground railway case, the IL based on overall velocity level is between -2 and 2 dB, rising to 4 dB for the box foundation. The IL for the pile foundation is one of the lowest, whereas in the surface railway case, it is the second highest.
6. When predicting train-induced ground vibration, the influence of adjacent building foundations should not be ignored. The present results provide a reference, but it can be expected that the effect will vary depending on the size of the building and the soil properties.

Acknowledgements

This work was supported by China Scholarship Council (No.202007090012).

Conflict of interest statement

No potential conflict of interest was reported by the authors.

References

1. Thompson, D.J., G. Kouroussis, and E. Ntotsios, *Modelling, simulation and evaluation of ground vibration caused by rail vehicles*. Vehicle System Dynamics, 2019. **57**(7): p. 936–983.

2. With, C., M. Bahrekazemi, and A. Bodare, *Validation of an empirical model for prediction of train-induced ground vibrations.* Soil Dynamics and Earthquake Engineering, 2006. **26**(11): p. 983–990.
3. Gjelstrup, H., et al., *Probabilistic empirical model for train-induced vibrations.* Proceedings of the Institution of Civil Engineers-Structures and Buildings, 2016. **169**(8): p. 563–573.
4. Kouroussis, G., K.E. Vogiatzis, and D.P. Connolly, *Assessment of railway ground vibration in urban area using in-situ transfer mobilities and simulated vehicle-track interaction.* International Journal of Rail Transportation, 2018. **6**(2): p. 113–130.
5. Alsharo, A., et al., *Investigating the effect of using softer rail-pads on ground-borne vibration from underground railways.* International Journal of Rail Transportation, 2024. **12**(5): p. 803–826.
6. *ISO 14837-1: Mechanical vibration—ground-borne noise and vibration arising from rail systems.* International Organization for Standardization, Geneva, Switzerland, 2005.
7. Hanson, C.E., et al., *High-speed ground transportation noise and vibration impact assessment*. 2012, United States Federal Railroad Administration. Office of Railroad Policy and Development.
8. Hanson, C., D. Towers, and L. Meister, *Transit noise and vibration impact assessment, Report FTA-VA-90-1003-06*. 2006, US Department of Transportation, Federal Transit Administration: Office of Planning and Environment.
9. Sheng, X., C. Jones, and D. Thompson, *A theoretical model for ground vibration from trains generated by vertical track irregularities.* Journal of sound and vibration, 2004. **272**(3-5): p. 937–965.
10. Hussein, M. and H. Hunt, *A numerical model for calculating vibration from a railway tunnel embedded in a full-space.* Journal of Sound and Vibration, 2007. **305**(3): p. 401–431.
11. Yang, J., et al., *A spatial train-track-tunnel coupled dynamics model for assessing influences of curved railway line on circular tunnel vibrations.* Applied Mathematical Modelling, 2025. **140**: p. 115892.
12. Yang, J., et al., *A 3D train-track-tunnel-soil coupled dynamics model based on semi-analytical cylindrical layer element.* Computers and Geotechnics, 2025. **179**: p. 106966.
13. Jin, Q., et al., *A 2.5D finite element and boundary element model for the ground vibration from trains in tunnels and validation using measurement data.* Journal of Sound and Vibration, 2018. **422**: p. 373–389.
14. Li, Z., et al., *2D and 3D soil finite/infinite element models: modelling, comparison and application in vehicle-track dynamic interaction.* International Journal of Rail Transportation, 2023. **11**(3): p. 339–363.
15. Xu, L., et al., *Further research of multi-scale assemble and matrix reassemble method for efficient analysis of railway track–substructure system subjected to a moving train.* Railway Engineering Science, 2025. **33**(2): p. 271–289.
16. Sheng, X., C.J.C. Jones, and D.J. Thompson, *Prediction of ground vibration from trains using the wavenumber finite and boundary element methods.* Journal of Sound and Vibration, 2006. **293**(3-5): p. 575–586.

17. Degrande, G., et al., *A numerical model for ground-borne vibrations from underground railway traffic based on a periodic finite element–boundary element formulation.* Journal of Sound and Vibration, 2006. **293**(3-5): p. 645–666.
18. François, S., et al., *A 2.5 D coupled FE–BE methodology for the dynamic interaction between longitudinally invariant structures and a layered halfspace.* Computer methods in applied mechanics and engineering, 2010. **199**(23-24): p. 1536–1548.
19. Xu, Q., et al., *Comparison of 2D and 3D prediction models for environmental vibration induced by underground railway with two types of tracks.* Computers and Geotechnics, 2015. **68**: p. 169–183.
20. Auersch, L., *Simple and fast prediction of train-induced track forces, ground and building vibrations.* Railway Engineering Science, 2020. **28**(3): p. 232–250.
21. Kuo, K.A., et al. *Applications of PiP: Vibration of embedded foundations near a railway tunnel*. in *7 th European Conference on Structural Dynamics (EURODYN)*. 2008.
22. Auersch, L., *Dynamic stiffness of foundations on inhomogeneous soils for a realistic prediction of vertical building resonance.* Journal of geotechnical and geoenvironmental engineering, 2008. **134**(3): p. 328–340.
23. Hussein, M., et al., *The use of sub-modelling technique to calculate vibration in buildings from underground railways.* Proceedings of the Institution of Mechanical Engineers, Part F: Journal of Rail and Rapid Transit, 2013. **229**(3): p. 303–314.
24. He, C., S. Zhou, and P. Guo, *An efficient three-dimensional method for the prediction of building vibrations from underground railway networks.* Soil Dynamics and Earthquake Engineering, 2020. **139**: p. 106269.
25. Clot, A., R. Arcos, and J. Romeu, *Efficient three-dimensional building-soil model for the prediction of ground-borne vibrations in buildings.* Journal of Structural Engineering, 2017. **143**(9): p. 04017098.
26. Yang, J., et al., *Prediction and mitigation of train-induced vibrations of large-scale building constructed on subway tunnel.* Science of The Total Environment, 2019. **668**: p. 485–499.
27. Ropars, P., X. Vuylsteke, and E. Augis. *Vibrations induced by metro in sensitive buildings; experimental and numerical comparisons*. in *EURONOISE 2018 Conference. Heraklion, Greece*. 2018.
28. Bucinskas, P., et al., *Modelling train-induced vibration of structures using a mixed-frame-of-reference approach.* Journal of Sound and Vibration, 2021. **491**: p. 115575.
29. Lopes, P., et al., *Numerical modeling of vibrations induced by railway traffic in tunnels: From the source to the nearby buildings*. Soil Dynamics and Earthquake Engineering, 2014. **61**: p. 269–285.
30. Lopes, P., et al., *Influence of soil stiffness on building vibrations due to railway traffic in tunnels: Numerical study.* Computers and Geotechnics, 2014. **61**: p. 277–291.
31. Colaço, A., et al., *Vibrations induced by railway traffic in buildings: Experimental validation of a sub-structuring methodology based on 2.5D FEM-MFS and 3D FEM.* Engineering Structures, 2021. **240**: p. 112381.
32. Villot, M., et al., *Modeling the influence of structural modifications on the response of a building to railway vibration.* Noise Control Engineering Journal, 2011. **59**(6): p. 641–651.

33. Coulier, P., et al., *Application of hierarchical matrices to boundary element methods for elastodynamics based on Green's functions for a horizontally layered halfspace.* Engineering Analysis with Boundary Elements, 2013. **37**(12): p. 1745–1758.
34. Çelebi, E., S. Fırat, and İ. Çankaya, *The evaluation of impedance functions in the analysis of foundations vibrations using boundary element method.* Applied Mathematics and Computation, 2006. **173**(1): p. 636–667.
35. Edirisinghe, T.L. and J.P. Talbot, *The significance of source-receiver interaction in the response of piled foundations to ground-borne vibration from underground railways.* Journal of Sound and Vibration, 2021. **506**: p. 116178.
36. Verbraken, H., G. Lombaert, and G. Degrande, *Verification of an empirical prediction method for railway induced vibrations by means of numerical simulations.* Journal of Sound and Vibration, 2011. **330**(8): p. 1692–1703.
37. Kuo, K., et al., *Hybrid predictions of railway induced ground vibration using a combination of experimental measurements and numerical modelling.* Journal of Sound and Vibration, 2016. **373**: p. 263–284.
38. Kouroussis, G., K.E. Vogiatzis, and D.P. Connolly, *A combined numerical/experimental prediction method for urban railway vibration.* Soil Dynamics and Earthquake Engineering, 2017. **97**: p. 377–386.
39. Colaço, A., et al., *Combination of experimental measurements and numerical modelling for prediction of ground-borne vibrations induced by railway traffic.* Construction and Building Materials, 2022. **343**: p. 127928.
40. Reumers, P., et al., *Integration of a hybrid vibration prediction model for railways into noise mapping software: methodology, assumptions and demonstration.* Railway Engineering Science, 2025. **33**(1): p. 1–26.
41. Lai, C.G., et al., *Prediction of railway-induced ground vibrations in tunnels.* Journal of vibration and acoustics, 2005. **127**(5): p. 503–514.
42. Liu, W., et al., *Prediction of ground-borne vibration induced by a moving underground train based on excitation experiments.* Journal of Sound and Vibration, 2022. **523**: p. 116728.
43. Li, Z., et al., *Hybrid method combining numerical modelling and experimental measurements for predicting ground-borne vibrations induced by underground trains.* Soil Dynamics and Earthquake Engineering, 2024. **187**: p. 108959.
44. Ntotsios, E., D.J. Thompson, and M.F.M. Hussein, *A comparison of ground vibration due to ballasted and slab tracks*. Transportation Geotechnics, 2019. **21**.
45. Ntotsios, E., D. Thompson, and M. Hussein, *The effect of track load correlation on ground-borne vibration from railways.* Journal of Sound and Vibration, 2017. **402**: p. 142–163.
46. Forrest, J.A. and H.E.M. Hunt, *A three-dimensional tunnel model for calculation of train-induced ground vibration.* Journal of Sound and Vibration, 2006. **294**(4-5): p. 678–705.
47. Forrest, J.A. and H.E.M. Hunt, *Ground vibration generated by trains in underground tunnels.* Journal of Sound and Vibration, 2006. **294**(4-5): p. 706–736.
48. Hussein, M., et al., *The fictitious force method for efficient calculation of vibration from a tunnel embedded in a multi-layered half-space.* Journal of sound and vibration, 2014.

333(25): p. 6996–7018.
49. Ntotsios, E., et al., *A track-independent vehicle indicator for ground-borne noise and vibration emission classification.* Transportation Geotechnics, 2024. **45**.
50. Thompson, D., et al., *Database for vibration emission, ground transmission and building transfer functions.* , in *SILVARSTAR project GA 101015442, Deliverable D2. 1, Report to the EC*. 2022.
51. Thompson, D., *Railway noise and vibration: mechanisms, modelling and means of control (second edition)*. 2024: Elsevier.
52. Lurcock, D., *Predicting groundborne noise and vibration in buildings from railway*, in *Faculty of Engineering and Environment*. 2018, University of Southampton. p. 346.